1

Electromechanical Dampers for Vibration Control of Structures and Rotors

Andrea Tonoli, Nicola Amati and Mario Silvagni
Mechanics Department, Mechatronics Laboratory - Politecnico di Torino
Italy

To the memory of Pietro, a model student, a first- class engineer, a hero

1. Introduction

Viscoelastic and fluid film dampers are the main two categories of damping devices used for the vibration suppression in machines and mechanical structures. Although cost effective and of small size and weight, they are affected by several drawbacks: the need of elaborate tuning to compensate the effects of temperature and frequency, the ageing of the material and their passive nature that does not allow to modify their characteristics with the operating conditions. Active or semi-active electro-hydraulic systems have been developed to allow some forms of online tuning or adaptive behavior. More recently, electrorheological, (Ahn et al., 2002), (Vance & Ying, 2000) and magnetorheological (Vance & Ying, 2000) semi-active damping systems have shown attractive potentialities for the adaptation of the damping force to the operating conditions. However, electro-hydraulic, electrorheological, and magnetorheological devices cannot avoid some drawbacks related to the ageing of the fluid and to the tuning required for the compensation of the temperature and frequency effects.

Electromechanical dampers seem to be a valid alternative to viscoelastic and hydraulic ones due to, among the others: a) the absence of all fatigue and tribology issues motivated by the absence of contact, b) the small sensitivity to the operating conditions, c) the wide possibility of tuning even during operation, and d) the predictability of the behavior. The attractive potentialities of electromechanical damping systems have motivated a considerable research effort during the past decade. The target applications range from the field of rotating machines to that of vehicle suspensions.

Passive or semi-active eddy current dampers have a simpler architecture compared to active closed loop devices, thanks to the absence of power electronics and position sensors and are intrinsically not affected by instability problems due to the absence of a fast feedback loop. The simplified architecture guarantees more reliability and lower cost, but allows less flexibility and adaptability to the operating conditions. The working principle of eddy current dampers is based on the magnetic interaction generated by a magnetic flux linkage's variation in a conductor (Crandall et al., 1968), (Meisel, 1984). Such a variation may be generated using two different strategies:

Source: Vibration Control, Book edited by: Dr. Mickaël Lallart,
ISBN 978-953-307-117-6, pp. 380, September 2010, Sciyo, Croatia, downloaded from SCIYO.COM

- moving a conductor in a stationary magnetic field that is variable along the direction of the motion;
- changing the reluctance of a magnetic circuit whose flux is linked to the conductor.

In the first case, the eddy currents in the conductor interact with the magnetic field and generate Lorenz forces proportional to the relative velocity of the conductor itself. In (Graves et al., 2000) this kind of damper are defined as "motional" or "Lorentz" type. In the second case, the variation of the reluctance of the magnetic circuit produces a time variation of the magnetic flux. The flux variation induces a current in the voltage driven coil and, therefore, a dissipation of energy. This kind of dampers is defined in (Nagaya, 1984) as "transformer", or "reluctance" type.

The literature on eddy current dampers is mainly focused on the analysis of "motional" devices. Nagaya in (Nagaya, 1984) and (Nagaya & Karube, 1989) introduces an analytical approach to describe how damping forces can be exploited using monolithic plane conductors of various shapes. Karnopp and Margolis in (Karnopp, 1989) and (Karnopp et al., 1990) describe how "Lorentz" type eddy current dampers could be adopted as semi-active shock absorbers in automotive suspensions. The application of the same type of eddy current damper in the field of rotordynamics is described in (Kligerman & Gottlieb, 1998) and (Kligerman et al., 1998).

Being usually less efficient than "Lorentz" type, "transformer" eddy current dampers are less common in industrial applications. However they may be preferred in some areas for their flexibility and construction simplicity. If driven with a constant voltage they operate in passive mode while if current driven they become force actuators to be used in active configurations. A promising application of the "transformer" eddy current dampers seems to be their use in aero-engines as a non rotating damping device in series to a conventional rolling bearing that is connected to the main frame with a mechanical compliant support. Similarly to a squeeze film damper, the device acts on the non rotating part of the bearing. As it is not rotating, there are no eddy currents in it due to its rotation but just to its whirling. The coupling effects between the whirling motion and the torsional behavior of the rotor can be considered negligible in balanced rotors (Genta, 2004).

In principle the behaviour of Active Magnetic Dampers (AMDs) is similar to that of Active Magnetic Bearings (AMBs), with the only difference that the force generated by the actuator is not aimed to support the rotor but just to supply damping. The main advantages are that in the case of AMDs the actuators are smaller and the system is stable even in open-loop (Genta et al., 2006),(Genta et al., 2008),(Tonoli et al., 2008). This is true if the mechanical stiffness in parallel to the electromagnets is large enough to compensate the negative stiffness induced by the electromagnets.

Classical AMDs work according to the following principle: the gap between the rotor and the stator is measured by means of position sensors and this information is then used by the controller to regulate the current of the power amplifiers driving the magnet coils. Self-sensing AMDs can be classified as a particular case of magnetic dampers that allows to achieve the control of the system without the introduction of the position sensors. The information about the position is obtained by exploiting the reversibility of the electromechanical interaction between the stator and the rotor, which allows to obtain mechanical variables from electrical ones.

The sensorless configuration leads to many advantages during the design phase and during the practical realization of the device. The intrinsic punctual collocation of the not present sensor avoids the inversion of modal phase from actuator to sensor, with the related loss of

the zero/pole alternation and the consequent problems of stabilization that may affect a sensed solution. Additionally, getting rid of the sensors leads to a reduction of the costs, the reduction of the cabling and of the overall weight.
The aim of the present work is to present the experience of the authors in developing and testing several electromagnetic damping devices to be used for the vibration control.
A brief theoretical background on the basic principles of electromagnetic actuator, based on a simplified energy approach is provided. This allow a better understanding of the application of the electromagnetic theory to control the vibration of machines and mechanical structures. According to the theory basis, the modelling of the damping devices is proposed and the evidences of two dedicated test rigs are described.

2. Description and modelling of electromechanical dampers

2.1 Electromagnetic actuator basics

Electromagnetic actuators suitable to develop active/semi-active/passive damping efforts can be classified in two main categories: Maxwell devices and Lorentz devices.
For the first, the force is generated due to the variation of the reluctance of the magnetic circuit that produces a time variation of the magnetic flux linkage. In the second, the damping force derives from the interaction between the eddy currents generated in a conductor moving in a constant magnetic field.

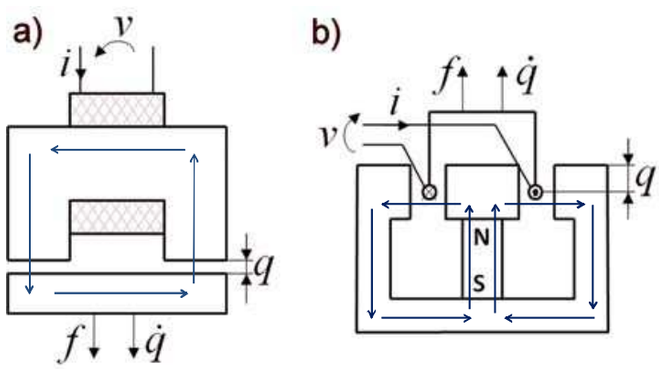

Fig. 1. Sketch of a) Maxwell magnetic actuator and b) Lorentz magnetic actuator.

For both (Figure 1), the energy stored in the electromagnetic circuit can be expressed by:

$$E = \int_{t_0}^{t_1} \left(P_{electrical} + P_{mechanical} \right) dt = \int_{t_0}^{t_1} \left(v(t) i(t) + f(t) \dot{q}(t) \right) dt \tag{1}$$

Where the electrical power ($P_{electrical}$) is the product of the voltage ($v(t)$) and the current ($i(t)$) flowing in the coil, and the mechanical power is the product of the force ($f(t)$) and speed ($\dot{q}(t)$) of the moving part of the actuator.
Considering the voltage ($v(t)$) as the time derivative of the magnetic flux linkage ($\lambda(t)$), eq.(1) can be written as:

$$E = \int_{t_0}^{t_1} \left(\frac{d\lambda(t)}{dt} i(t) + f(t) \dot{q}(t) \right) dt = \int_{\lambda_0}^{\lambda_1} i(t) d\lambda + \int_{q_0}^{q_1} f(t) dq = E_\lambda + E_q \tag{2}$$

In the following steps, the two terms of the energy E will be written in explicit form. With reference to Maxwell Actuator, Figure 1a, the Ampère law is:

$$H_a l_a + H_{fe} l_{fe} = Ni \tag{3}$$

where H_a and H_{fe} indicate the magnetic induction in the airgap and in the iron core while l_a and l_{fe} specify the length of the magnetic circuit flux lines in the airgap in the same circuit. The product Ni is the total current linking the magnetic flux (N indicates the number of turns while i is the current flowing in each wire section). If the magnetic circuit is designed to avoid saturation into the iron, the magnetic flux density B can be related to magnetic induction by the following expression:

$$B = \mu_0 H \quad , \quad B = \mu_0 \mu_{fe} H_{fe} \, . \tag{4}$$

Considering that ($\mu_{fe} >> \mu_0$) and noting that the total length of the magnetic flux lines in the airgap is twice q, eq.(3) can be simply written as:

$$\frac{2Bq}{\mu_0} = Ni \, . \tag{5}$$

The expressions of the magnetic flux linking a single turn and the total number of turns in the coil are respectively:

$$\varphi = BS_{airgap} \tag{6}$$

$$\lambda = N\varphi = NBS_{airgap} = \mu_0 \frac{N^2 S_{airgap}}{2q} i \tag{7}$$

Hence, knowing the expression (eq.(7)) of the total magnetic flux leakage, the E_λ of eq. (1) for a generic flux linkage λ and air q, can be computed as:

$$E_\lambda = \int_{\lambda_0}^{\lambda_1} i(t) d\lambda = \frac{\lambda^2 q}{\mu_0 N^2 S_{airgap}} \tag{8}$$

Note that this is the total contribution to the energy (E) if no external active force is applied to the moving part.
Finally, the force generated by the actuator and the current flowing into the coil can be computed as:

$$f = \frac{\partial E}{\partial q} = \frac{\lambda^2}{\mu_0 N^2 S_{airgap}} \, , \tag{9}$$

$$i = \frac{\partial E}{\partial \lambda} = \frac{2q\lambda}{\mu_0 N^2 S_{airgap}} \, . \tag{10}$$

Then, the force relative to the current can be obtained by substituting eq.(10) into eq.(9):

$$f = \frac{\mu_0 N^2 S_{airgap} i^2}{4q^2} . \tag{11}$$

Considering the **Lorentz actuator** (Figure 1 b**)**, if the coil movement q is driven while the same coil is in open circuit configuration so that no current flows in the coil, the energy (*E*) is zero as both the integrals in eq. (1) are null. In the case the coil is in a constant position and the current flow in it varies from zero to a certain value, the contribution of the integral leading to (E_q) is null as the displacement of the anchor (*q*) is constant while the integral leading to (E_λ) can be computed considering the total flux leakage.

$$\lambda = 2\pi RqB + Li = \lambda_0 + Li \tag{12}$$

The first term is the contribution of the magnetic circuit (R is the radius of the coil, q is the part of the coil in the magnetic field), while the second term is the contribution to the flux of the current flowing into the coil. Current can be obtained from eq.(12) as:

$$i = \frac{\lambda - \lambda_0}{L} \tag{13}$$

Hence, from the expression of eq.(13), the E_λ term, that is equal to the total energy, can be computed as:

$$E_\lambda = \int_{\lambda_0}^{\lambda_1} i(t) d\lambda = \int_{\lambda_0}^{\lambda_1} \frac{\lambda - \lambda_0}{L} d\lambda = \frac{1}{2L}(\lambda - \lambda_0)^2 = \frac{1}{2L}(\lambda - 2\pi RqB)^2 \tag{14}$$

Finally computing the derivative with respect to the displacement and to the flux, the force generated by the actuator and the current flowing into the coil can be computed:

$$f = \frac{\partial E}{\partial q} = \frac{-2\pi RB}{L}(\lambda - \lambda_0) \tag{15}$$

$$i = \frac{\partial E}{\partial \lambda} = \frac{1}{L}(\lambda - \lambda_0) \tag{16}$$

The expression of the force relative to the current can be obtained by substituting eq.(16) into eq.(15)

$$f = -2\pi RBi . \tag{17}$$

The equations above mentioned represent the basis to understand the behaviour of electromagnetic actuators adopted to damp the vibration of structures and machines.

2.2 Classification of electromagnetic dampers

Figure 2 shows a sketch representing the application of a Maxwell type and a Lorentz type actuator. In the field of damping systems the former is named transformer damper while the latter is called motional damper. The transformer type dampers can operate in active mode if current driven or in passive mode if voltage driven. The drawings evidence a compliant

supporting device working in parallel to the damper. In the specific its role is to support the weight of the rotor and supply the requested compliance to exploit the performance of the damper (Genta, 2004). Note that the sketches are referred to an application for rotating systems. The aim in this case is to damp the lateral vibration of the rotating part but the concept can be extended to any vibrating device. In fact, the damper interacts with the non rotating raceway of the bearing that is subject only to radial vibration motion.

2.3 Motional eddy current dampers

The present section is devoted to describe the equations governig the behavior of the motional eddy current dampers. A torsional device is used as reference being the linear ones a subset. The reference scheme (Kamerbeek, 1973) is a simplified induction motor with one magnetic pole pair (Figure 3a).

The rotor is made by two windings 1,1′ and 2,2′ installed in orthogonal planes. It is crossed by the constant magnetic field (flux density $\mathbf{B}_s$) generated by the stator. The analysis is performed under the following assumptions:

- the two rotor coils have the same electric parameters and are shorted.
- The reluctance of the magnetic circuit is constant. The analysis is therefore only applicable to motional eddy current devices and not to transformer ones (Graves et al., 2009), (Tonoli et al., 2008).

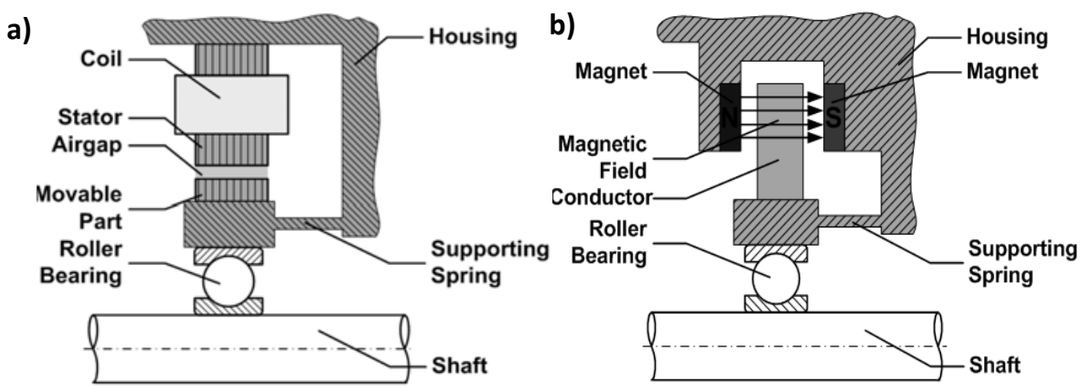

Fig. 2. Sketch of a transformer (a) and a motional damper (b).

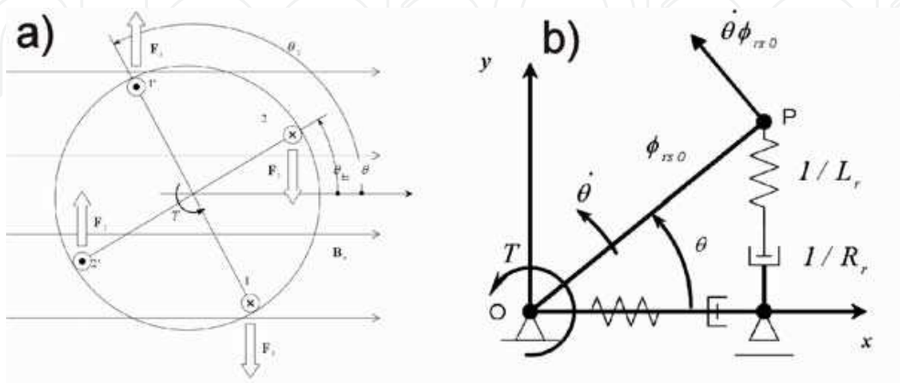

Fig. 3. a) Sketch of the induction machine b) Mechanical analogue. The torque T is balanced by the force applied to point P by the spring-damper assemblies.

- The magnetic flux generated by the stator is constant as if it were produced by permanent magnets or by current driven electromagnets.
- The stator is assumed to be fixed. This is equivalent to describe the system in a reference frame rigidly connected to it.
- All quantities are assumed to be independent from the axial coordinate.
- Each of the electric parameter is assumed to be lumped.

Angle $\theta(t)$ between the plane of winding 2 and the direction of the magnetic field indicates the angular position of the rotor relative to the stator. When currents i_{r1} and i_{r2} flow in the windings, they interact with the magnetic field of the stator and generate a pair of Lorentz forces ($F_{1,2}$ in Figure 3a). Each force is perpendicular to both the magnetic field and to the axis of the conductors. They are expressed as:

$$F_1 = Nl_r i_{r1} B_s, \qquad F_2 = Nl_r i_{r2} B_s \tag{18}$$

where N and l_r indicate the number of turns in each winding and their axial length. The resulting electromagnetic torques T_1 and T_2 applied to the rotor of diameter d_r are:

$$T_1 = F_1 d_r \sin\theta = \phi_{rs0} \sin\theta \, i_{r1}, \qquad T_2 = F_2 d_r \cos\theta = \phi_{rs0} \cos\theta \, i_{r2} \tag{19}$$

where $\phi_{rs0} = Nl_r d_r B_s$ is the magnetic flux linked with each coil when its normal is aligned with the magnetic field $\mathbf{B}_s$. It represents the maximum magnetic flux. The total torque acting on the rotor is:

$$T = T_1 + T_2 = \phi_{rs0} \left(\sin\theta \, i_{r1} + \cos\theta \, i_{r2} \right) \tag{20}$$

Note that the positive orientation of the currents indicated in Figure 3a has been assumed arbitrarily, the results are not affected by this choice.

From the mechanical point of view the eddy current damper behaves then as a crank of radius ϕ_{rs0} whose end is connected to two spring/damper series acting along orthogonal directions. Even if the very concept of mechanical analogue is usually a matter of elementary physics textbooks, the mechanical analogue of a torsional eddy current device is not common in the literature. It has been reported here due to its practical relevance. Springs and viscous dampers can in fact be easily assembled in most mechanical simulation environments. The mechanical analogue in Figure 3b allows to model the effect of the eddy current damper without needing a multi-domain simulation tool.

The model of an eddy current device with p pole pairs can be obtained by considering that each pair involves two windings electrically excited with 90^o phase shift. For a one pole pair device, each pair is associated with a rotor angle of 2π rad; a complete revolution of the rotor induces one electric excitation cycle of its two windings. Similarly, for a p pole pairs device, each pair is associated to a $2\pi / p$ rad angle, a complete revolution of the rotor induces then p excitation cycles on each winding ($\theta_e = p\theta$).

The orthogonality between the two windings allows adopting a complex flux linkage variable

$$\phi_r = \phi_{r1} + j\phi_{r2} \tag{21}$$

where j is the imaginary unit. Similarly, also the current flowing in the windings can be written as $i_r = i_{r1} + j i_{r2}$. The total magnetic flux ϕ_r linked by each coil is contributed by the

currents i_r through the self inductance L_r and the flux generated by the stator and linked to the rotor

$$\phi_r = L_r i_r + \frac{\phi_{rs0}}{p} e^{-j\theta_e} . \tag{22}$$

The differential equation governing the complex flux linkage ϕ_r is obtained by substituting eq.(22) in the Kirchoff's voltage law

$$\frac{d\phi_r}{dt} + R_r i_r = 0 . \tag{23}$$

It is therefore expressed as

$$\dot{\phi}_r + \omega_p \phi_r = j\dot{\theta}\phi_{rs0} e^{-j\theta_e} \tag{24}$$

where ω_p is the is the electrical pole of each winding

$$\omega_p = \frac{R_r}{L_r} . \tag{25}$$

The electromagnetic torque of eq.(20) results to be p times that of a single pole pair

$$T = p \frac{\phi_{rs0}}{L_r} Im\left(\phi_r e^{j\theta_e}\right) . \tag{26}$$

The model holds under rather general input angular speed. The mechanical torque will be determined for the following operating conditions:

- coupler: the angular speed is constant: $\dot{\theta} = \Omega = \text{const}$,
- damper: the rotor is subject to a small amplitude torsional vibration relative to the stator.

Coupler

For constant rotating speed ($\dot{\theta}(t) = \Omega$, $\theta(t) = \Omega t$), the steady state solution of eq.(24) is

$$\phi_r = \phi_{r0} e^{-jp\Omega t}; \qquad \phi_{r0} = \frac{j\Omega\phi_{rs0}}{\omega_p - jp\Omega} \tag{27}$$

The torque (T) to speed (Ω) characteristic is found by substituting eq.(27) into eq.(26). The result is the familiar torque to slip speed expression of an induction machine running at constant speed

$$T(\Omega) = \frac{c_0}{1 + (p\Omega)^2 / \omega_p^2} \Omega, \qquad \text{where } c_0 = \frac{p\phi_{rs0}^2}{R_r} . \tag{28}$$

A simple understanding of this characteristic can be obtained by referring to the mechanical analogue of Figure 3b. At speeds such that the excitation frequency is lower than the pole ($p\Omega << \omega_p$), the main contribution to the deformation is that of the dampers, while the

springs behave as rigid bodies. The resultant force vector acting on point P is due to the dampers and acts perpendicularly to the crank ϕ_{rs0}, this produces a counteracting torque

$$T = c_0 \Omega \tag{29}$$

By converse, at speeds such that $p\Omega >> \omega_p$ the main contribution to the deformation is that of the springs, while the dampers behave as rigid bodies. The resultant force vector on point P is due to the springs. It is oriented along the crank ϕ_{rs0} and generates a null torque.

Damper

If the rotor oscillates ($\theta(t) = \theta_0 \Re e(e^{j\omega t}) + \theta_m$) with small amplitude about a given angular position θ_m, the state eq.(24) can be linearized resorting to the small angle assumption

$$\dot{\phi}_r + \omega_p \phi_r = j\dot{\theta}\phi_{rs0} e^{-jp\theta_m} \tag{30}$$

The solution is found in terms of the transfer function between the rotor flux $\phi_r(s)$ and the input speed $\dot{\theta}(s)$

$$\frac{\phi_r(s)}{\dot{\theta}(s)} = \frac{j\phi_{rs0} e^{-jp\theta_m}}{s + \omega_p}, \tag{31}$$

where s is the Laplace variable. The mechanical impedance $Z_m(s)$, i.e. the torque to speed transfer function is found by substituting eq.(31) into Eq.(26)

$$Z_m(s) = \frac{T(s)}{\dot{\theta}(s)} = \frac{c_{em}}{1 + s/\omega_p} = \frac{c_{em}}{1 + s(k_{em}/c_{em})}. \tag{32}$$

This impedance is that of the series connection of a torsional damper and a torsional spring with viscous damping and spring stiffness given by

$$c_{em} = \frac{p\phi_{rs0}^2}{R_r}, \qquad k_{em} = \frac{p\phi_{rs0}^2}{L_r} \tag{33}$$

that are constant parameters. At low frequency ($s << \omega_p$), the device behaves as a pure viscous damper with coefficient c_{em}. This is the term that is taken into account in the widespread reactive model. At high frequency ($s >> \omega_p$) it behaves as a mechanical linear spring with stiffness k_{em}. This term on the contrary is commonly neglected in all the models presented in the literature (Graves et al., 2009), (Nagaya, 1984), (Nagaya & Karube, 1989). The bandwidth of the mechanical impedance (Figure 4b) is due to the electrical circuit resistance and inductance. It must be taken into account for the design of eddy current dampers. The assumption of neglecting the inductance is valid only for frequency lower than the electric pole ($s << \omega_p$). The behavior of the mechanical impedance has effects also on the operation of an eddy current coupler. Due to the bandwidth limitations, it behaves as a low pass filter for each frequency higher than the electric pole.

To correlated the torque to speed characteristic of eq.(28) and the mechanical impedance of eq. (32), it shold be analized that the slope c_0 of the torque to speed characteristic at zero or low speed ($\Omega = p\omega_p$) is equal to the mechanical impedance at zero or low frequency ($s = \omega_p$):

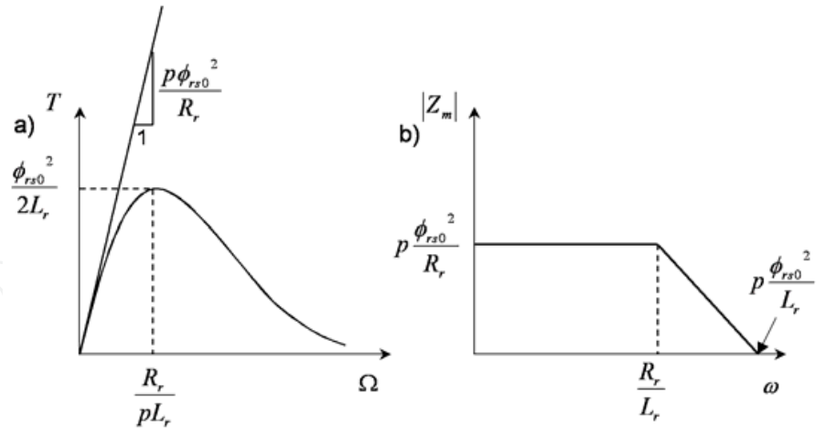

Fig. 4. a) Static characteristic of an axial-symmetric induction machine b) Representation of its mechanical impedance (magnitude in logarithmic scales).

$$c_0 = c_{em} = \frac{p\phi_{rs0}^2}{R_r}. \tag{34}$$

Additionally, the maximum torque ($T_{\max}$) at steady state is related to the high frequency mechanical impedance ($Z_m(s)$)

$$T_{\max} = \frac{\phi_{rs0}^2}{2L_r}, \; k_{em} = \frac{p\phi_{rs0}^2}{L_r} \tag{35}$$

The relationship between $T_{\max}$ and $Z_m(s)$ at high frequency is therefore

$$\Omega_{T_{\max}} = \frac{\omega_p}{p}, \qquad T_{\max} = \frac{c_{em}\omega_p}{2p} = \frac{k_{em}}{2p} \tag{36}$$

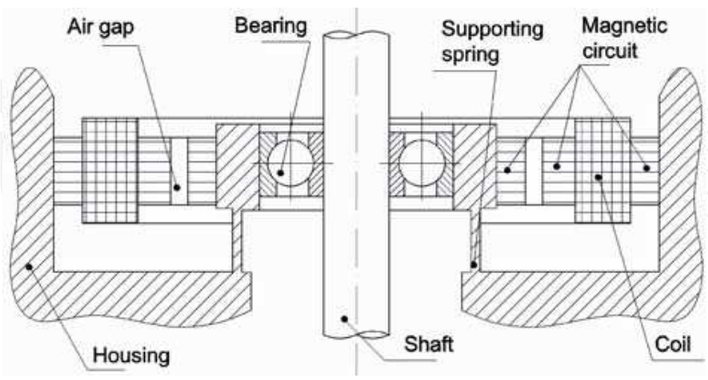

Fig. 5. Sketch of an Active Magnetic Damper in conjunction with a mechanical spring. They both act on the non rotating part of the bearing.

A graphical representation of the relationships between eqs.(35) and (36) is given in Figure 4. They allow to obtain the mechanical impedance and/or the state space model valid under general operating condition, eq.(24), from the torque to speed characteristic. This is of

interest because numerical tools performing constant speed analysis are far more common and consolidated than those dealing with transient analysis. Vice versa, the steady state torque to speed characteristic can be simply obtained identifying by vibration tests the parameters c_{em} and k_{em} (or ω_p).
It's worth to note that eqs.(28), (32) and Eqs.(35), (36) hold in general for eddy current devices with one or more pole pairs. They can be applied also to linear electric machies provided that the rotational degree of freedom is transformed into a linear one.

2.4 Transformer dampers in active mode (AMD)

Transformer dampers can be used in active mode. Active Magnetic Dampers (Figure 5) work in the same way as active magnetic bearings, with the only difference that in this case the force generated by the actuator is not aimed to support the rotor but, in the simplest control strategy, it may be designed just to supply damping; this doesn't exclude the possibility to develop any more complex control strategy. An AMD can be integrated into one of the supports of the rotor. In this concept, a rolling element bearing is supported in the housing via mechanical springs providing the required stiffness. Both the spring and the damper act on the non-rotating part of the support. The stiffness and the load bearing capacity is then provided by the mechanical device while the AMD is used to control the vibrations, adding damping, in its simplest form. It is important to note that the stiffness of the springs can be used to compensate the open loop negative stiffness of a typical Maxwell actuator. This allows to relieve the active control of the task to guarantee the static stability of the system. A proportional-derivative feedback loop based on the measurement of the support displacements may be enough to control the rotor vibrations. Sensors and a controller are then required to this end. Under the assumption of typical Maxwell actuators, the force that each coil of the actuator exerts on the moving part is computed by eq.(11), that can be used to design the actuators once its maximum control force is specified. It's worth to note that such damping devices can be applied to any vibrating system.

2.5 Transformer dampers in active mode and self-sensing operation

The reversibility of the electromechanical interaction induces an electrical effect when the two parts of an electromagnet are subject to relative motion (back electromotive force). This effect can be exploited to estimate mechanical variables from the measurement of electrical ones. This leads to the so-called self-sensing configuration that consists in using the electromagnet either as an actuator and a sensor. This configuration permits lower costs and shorter shafts (and thus higher bending frequencies) than classical configurations provided with sensors and non-collocation issues are avoided. In practice, voltage and current are used to estimate the airgap. To do so, the two main approaches are: the state-space observer approach (Vischer & Bleuler, 1990), (Vischer & Bleuler, 1993) and the airgap estimation using the current ripple (Noh & Maslen, 1997), (Schammass et al., 2005). The former is based on the electromechanical model of the system. As the resulting model is fully observable and controllable, the position and the velocity of the mechanical part can be estimated and fed back to control the vibrations of the system. This approach is applicable for voltage-controlled (Mizuno et al., 1996) and current-controlled (Mizuno et al., 1996) electromagnets. The second approach takes advantage from the current ripple due to the switching amplifiers to compute in real-time the inductance, and thus the airgap. The airgap-estimation can be based on the ripple slope (PWM driven amplifiers, (Okada et al., 1992)) or

on the ripple frequency (hysteresis amplifiers, (Mizuno et al., 1998)). So far in the literature, self-sensing configurations have been mainly used to achieve the complete suspension of the rotor. The poor robustness of the state-space approach greatly limited its adoption for industrial applications. As a matter of fact, the use of a not well tuned model results in the system instability (Mizuno et al., 1996) , (Thibeault & Smith 2002). Instead, the direct airgap estimation approach seems to be more promising in terms of robustness (Maslen et al., 2006).

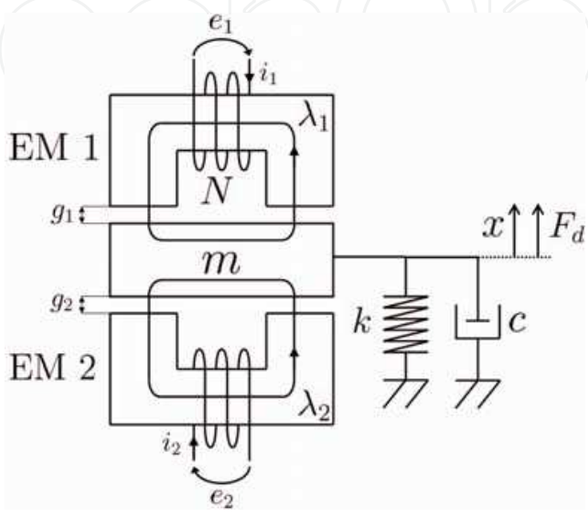

Fig. 6. Schematic model of electromagnets pair to be used for self-sensing modelling.

Here below is described a one degree of freedom mass-spring oscillator actuated by two opposite electromagnets (Figure 6). Parameters m, k and c are the mass, stiffness and viscous damping coefficient of the mechanical system. The electromagnets are assumed to be identical, and the coupling between the two electromagnetic circuits is neglected. The aim of the mechanical stiffness is to compensate the negative stiffness due to the electromagnets.
Owing to Newton's law in the mechanical domain, the Faraday and Kirchoff laws in the electrical domain, the dynamics equations of the system are:

$$\begin{aligned} m\ddot{x} + c\dot{x} + kx + F_1 + F_2 &= F_d \\ \dot{\lambda}_1 + Ri_1 &= v_1 \\ \dot{\lambda}_2 + Ri_2 &= v_2 \end{aligned} \tag{37}$$

where R is the coils resistance and v_j is the voltage applied to electromagnet j. F_d is the disturbance force applied to the mass, while F_1 and F_2 are the forces generated by the coils as in eq. (9).
The system dynamics is linearized around a working point corresponding to a bias voltage v_0 imposed to both the electromagnets:

$$\begin{aligned} i_j &= i_0 \pm i_c \\ v_j &= v_0 \pm v_c \,,\; j = 1,2 \\ F_j\left(i_j, x\right) &= \pm F_0 + \Delta F_j \end{aligned} \tag{38}$$

where F_0 is the initial force generated by the electromagnets due to the current $i_0 = v_0 / R$, and ΔF_j is the small variation of the electromagnets' forces. As the electromagnets are identical, $(i_1 - i_0) = -(i_2 - i_0) = i_c$. Therefore, a three-state-space model is used to study the four-state system dynamics described in eq.(37) (Vischer & Bleuler, 1990). The resulting linearized state-space model is:

$$\begin{aligned} X &= AX + Bu \\ y &= CX \end{aligned} \tag{39}$$

where *A*, *B* and *C* are the dynamic, action and output matrices respectively defined as:

$$A = \begin{bmatrix} 0 & 1 & 0 \\ -\dfrac{k + 2k_x}{m} & -\dfrac{c}{m} & \dfrac{2k_i}{m} \\ 0 & -\dfrac{k_m}{L_0} & -\dfrac{R}{L_0} \end{bmatrix},$$

$$B = \begin{bmatrix} 0 & 0 \\ \dfrac{1}{m} & 0 \\ 0 & \dfrac{1}{L_0} \end{bmatrix}, C = \begin{bmatrix} 0 & 0 & 1 \end{bmatrix}, \tag{40}$$

with the associated state, input and output vectors $X = \{x, \dot{x}, i_c\}^T$, $u = \{F_d, v_c\}^T$ $y = i_c$.

The terms in the matrices derive from the linearization of the non-linear functions defined in eq. (7) and eq. (9):

$$\begin{aligned} L_0 &= \frac{\Gamma}{x_0}, \quad k_m = L_0 \frac{i_0}{x_0}, \\ k_i &= L_0 \frac{i_0}{x_0}, \quad k_x = -k_m \frac{i_0}{x_0} \end{aligned} \tag{41}$$

where $\Gamma = \mu_0 N^2 S / 2$ is the characteristic factor of the electromagnets , L_0, k_i, k_m and k_x are the inductance, the current-force factor, the back-electromotive force factor, and the so-called negative stiffness of one electromagnet, respectively. The open-loop system is stable as long as the mechanical stiffness is larger than the total negative stiffness, i.e. $k + 2k_x > 0$. As eq.(39) describes the open-loop dynamics of the system for small variations of the variables, and the system stability is insured, the various coefficients of *A* can be identified experimentally.

Due to the strong nonlinearity of the electromagnetic force as a function of the displacement and the applied voltage, and to the presence of end stops that limit the travel of the moving

mass, the linear approach may seem to be questionable. Nevertheless, the presence of a mechanical stiffness large enough to overcome the negative stiffness of the electromagnets makes the linearization point stable, and compels the system to oscillate about it. The selection of a suitable value of the stiffness k is a trade-off issue deriving from the application requirements. However, as far as the linearization is concerned, the larger is the stiffness k relative to $|k_x|$, the more negligible the nonlinear effects become.

2.5.1 Control design

The aim of the present section is to describe the design strategy of the controller that has been used to introduce active magnetic damping into the system. The control is based on the Luenberger observer approach (Vischer & Bleuler, 1993), (Mizuno et al., 1996). The adoption of this approach was motivated by the relatively low level of noise affecting the current measurement. It consists in estimating in real time the unmeasured states (in our case, displacement and velocity) from the processing of the measurable states (the current). The observer is based on the linearized model presented previously, and therefore the higher frequency modes of the mechanical system have not been taken into account. Afterwards, the same model is used for the design of the state-feedback controller.

2.5.2 State observer

The observer dynamics is expressed as (Luenberger, 1971):

$$\dot{\hat{X}} = A\dot{X} + Bu + L\left(y - \hat{y}\right) \tag{42}$$

where $\hat{X}$ and $\hat{y}$ are the estimations of the system state and output, respectively. Matrix L is commonly referred to as the gain matrix of the observer. Eq.(42) shows that the inputs of the observer are the measurement of the current (y) and the control voltage imposed to the electromagnets (u).

The dynamics of the estimation error ε are obtained combining eq. (39) and eq. (42):

$$\dot{\varepsilon} = \left(A - LC\right)\varepsilon \tag{43}$$

where $\varepsilon = X - \hat{X}$. Eq. (43) emphasizes the role of L in the observer convergence. The location of the eigenvalues of matrix $\left(A - LC\right)$ on the complex plane determines the estimation time constants of the observer: the deeper they are in the left-half part of the complex plane, the faster will be the observer. It is well known that the observer tuning is a trade-off between the convergence speed and the noise rejection (Luenberger, 1971). A fast observer is desirable to increase the frequency bandwidth of the controller action. Nevertheless, this configuration corresponds to high values of L gains, which would result in the amplification of the unavoidable measurement noise y, and its transmission into the state estimation. This issue is especially relevant when switching amplifiers are used. Moreover, the transfer function that results from a fast observer requires large sampling frequencies, which is not always compatible with low cost applications.

2.5.3 State-feedback controller

A state-feedback control is used to introduce damping into the system. The control voltage is computed as a linear combination of the states estimated by the observer, with K as the control gain matrix. Owing to the separation principle, the state-feedback controller is designed considering the eigenvalues of matrix (A-BK).

Similarly to the observer, a pole placement technique has been used to compute the gains of K, so as to maintain the mechanical frequency constant. By doing so, the power consumption for damping is minimized, as the controller does not work against the mechanical stiffness. The idea of the design was to increase damping by shifting the complex poles closer to the real axis while keeping constant their distance to the origin ($|p_1| = |p_2| = constant$).

2.6 Semi-active transformer damper

Figure 7 shows the sketch of a "transformer" eddy current damper including two electromagnets. The coils are supplied with a constant voltage and generate the magnetic field linked to the moving element (anchor). The displacement with speed $\dot{q}$ of the anchor changes the reluctance of the magnetic circuit and produces a variation of the flux linkage. According to Faraday's law, the time variation of the flux generates a back electromotive force. Eddy currents are thus generated in the coils. The current in the coils is then given by two contributions: a fixed one due to the voltage supply and a variable one induced by the back electromotive force. The first contribution generates a force that increases with the decreasing of the air-gap. It is then responsible of a negative stiffness. The damping force is generated by the second contribution that acts against the speed of the moving element.

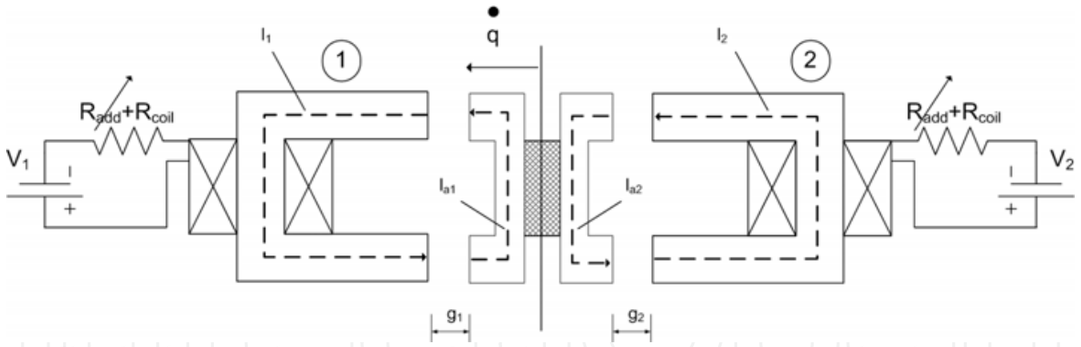

Fig. 7. Sketch of a two electromagnet Semi Active Magnetic Damper (the elastic support is omitted).

According to eq. (9), considering the two magnetic flux linkages λ_1 and λ_2 of both counteracting magnetic circuits, the total force acting on the anchor of the system is:

$$f = \frac{\lambda_2^2 - \lambda_1^2}{\mu_0 N^2 S_{airgap}} \tag{44}$$

The state equation relative to the electric circuit can be derived considering a constant voltage supply common for both the circuits that drive the derivative of the flux leakage and the voltage drop on the total resistance of each circuit $R=R_{coil}+R_{add}$ (coil resistance and additional resistance used to tune the electrical circuit pole as:

$$\begin{aligned}\dot{\lambda}_1 + \alpha R\left(g_0 - q\right)\lambda_1 &= V \\ \dot{\lambda}_2 + \alpha R\left(g_0 + q\right)\lambda_2 &= V\end{aligned} \tag{45}$$

Where g_0 is the nominal airgap and $\alpha = 2/(\mu_0 N^2 A)$.

Eqs.(44) and (45) are linearized for small displacements about the centered position of the anchor ($q = 0$) to understand the system behavior in terms of poles and zero structure

$$\begin{aligned}\dot{q} &= v, \\ \dot{\lambda}_1' &= -\alpha R\left(g_0\lambda_1' - \lambda_0 q\right), \\ \dot{\lambda}_2' &= -\alpha R\left(g_0\lambda_2' + \lambda_0 q\right),\end{aligned} \tag{46}$$

$$F_{em} = \alpha\lambda_0\left(\lambda_2' - \lambda_1'\right). \tag{47}$$

The term $\lambda_0 = V/\left(\alpha g_0 R\right)$ represents the magnetic flux linkage in the two electromagnets at steady state in the centered position as obtained from eq.(45) while λ_1' and λ_2' indicate the variation of the magnetic flux linkages relative to λ_0.

The transfer function between the speed $\dot{q}$ and the electromagnetic force F shows a first order dynamic with the pole (ω_{RL}) due to the R-L nature of the circuits

$$\begin{aligned}&\frac{F_{em}}{\dot{q}} = \frac{1}{s}\frac{K_{em}}{\left(1 + s/\omega_{RL}\right)}, \\ &\left(K_{em} = -\frac{2V^2/R}{g_0^2\omega_{RL}}, \quad \omega_{RL} = \frac{R}{L_0},\ L_0 = \frac{\mu_0 N^2 A}{2g_0}\right).\end{aligned} \tag{48}$$

L_0 indicates the inductance of each electromagnet at nominal airgap.

The mechanical impedance is a band limited negative stiffness. This is due to the factor $1/s$ and the negative value of K_{em} that is proportional to the electrical power ($K_m \geq -K_{em}$) dissipated at steady state by the electromagnet.

The mechanical impedance and the pole frequency are functions of the voltage supply V and the resistance R whenever the turns of the windings (N), the air gap area (A) and the airgap (g_0) have been defined. The negative stiffness prevents the use of the electromagnet as support of a mechanical structure unless the excitation voltage is driven by an active feedback that compensates it. This is the principle at the base of active magnetic suspensions.

A very simple alternative to the active feedback is to put a mechanical spring in parallel to the electromagnet. In order to avoid the static instability, the stiffness K_m of the added spring has to be larger than the negative electromechanical stiffness of the damper ($K_m \geq -K_{em}$). The mechanical stiffness could be that of the structure in the case of an already supported structure. Alternatively, if the structure is supported by the dampers themselves, the springs have to be installed in parallel to them. As a matter of fact, the mechanical spring in parallel to the transformer damper can be considered as part of the damper.

Due to the essential role of that spring, the impedance of eq.(48) is not very helpful in understanding the behavior of the damper. Instead, a better insight can be obtained by studying the mechanical impedance of the damper in parallel to the mechanical spring:

$$\frac{F_{em}}{v} = \frac{1}{s}\left(\frac{K_{em}}{\left(1+s/\omega_{RL}\right)} + K_m\right) = \frac{K_{eq}}{s}\frac{1+s/\omega_z}{1+s/\omega_{RL}} \qquad \text{where } K_{eq} = K_m + K_{em};\ \omega_z = \omega_{RL}\frac{K_{eq}}{K_m}. \tag{49}$$

Apart from the pole at null frequency, the impedance shows a zero-pole behavior. To ensure stability ($0 < -K_{em} < K_m$), the zero frequency (ω_z) results to be smaller than the pole frequency ($0 < \omega_z < \omega_{RL}$).

Figure 8a underlines that it is possible to identify three different frequency ranges:

1. Equivalent stiffness range ($\omega << \omega_z < \omega_{RL}$): the system behaves as a spring of stiffness $K_{eq} > 0$.
2. Damping range ($\omega_z < \omega < \omega_{RL}$): the system behaves as a viscous damper of coefficient

$$C = \frac{K_m}{\omega_{RL}} \tag{50}$$

3. Mechanical stiffness range ($\omega_z < \omega_{RL} << \omega$): the transformer damper contribution vanishes and the only contribution is that of the mechanical spring (K_m) in series to it.

A purely mechanical equivalent of the damper is shown in Figure 8b where a spring of stiffness K_{eq} is in parallel to the series of a viscous damper of coefficient *C* and a spring of stiffness $-K_{em}$. Due to the negative value of the electromagnetic stiffness, $-K_{em}$ is positive. It is interesting to note that the resulting model is the same as Maxwell's model of viscoelastic materials. At low frequency the system is dominated by the spring K_{eq} while the lower branch of the parallel connection does not contribute. At high frequency the viscous damper "locks" and the stiffnesses of the two springs add. The viscous damping dominates in the intermediate frequency range.

Eq. (50) shows that the product of the damping coefficient *C* and the pole frequency ω_{RL} is equal to the mechanical spring stiffness K_m. A sort of constant gain-bandwidth product therefore characterizes the damping range of the electromechanical damper. This product is just a function of the spring stiffness included in the damper. The constant gain-bandwidth means that for a given electromagnet, an increment of the added resistance leads to a higher pole frequency (eq. (48)) but reduces the damping coefficient of the same amount. Another interesting feature of the mechanical impedance of eq. (49) is that the only parameters affected by the supply voltage *V* are the equivalent stiffness (K_{eq}) and the zero-frequency (ω_z). The damping coefficient (*C*) and the pole frequency (ω_{RL}) are independent of it.

The substitution of the electromechanical stiffness K_{em} of eq. (48) into eq. (49) gives the zero frequency as function of the excitation voltage

$$\omega_z = \omega_{RL}\left(1 - \frac{2V^2/R}{g_0^2\omega_{RL}K_m}\right). \tag{51}$$

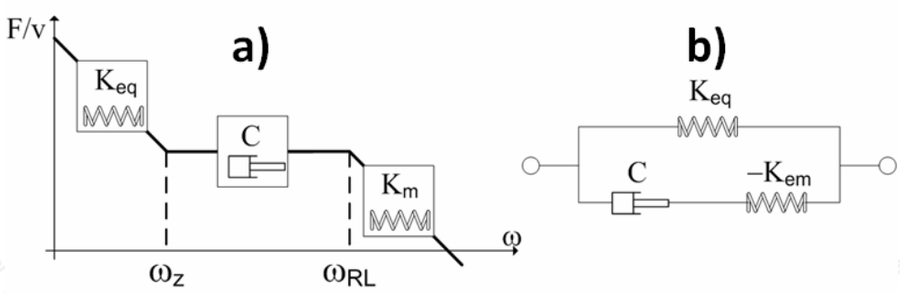

Fig. 8. a) mechanical impedance of a transformer eddy current damper in parallel to a spring of stiffness K_m. b) Mechanical equivalent.

The larger the supply voltage the smaller the zero frequency and the larger the width of the damping region. If V=0, there are no electromagnetic forces and the damper reduces to the mechanical spring. The outcome on the mechanical impedance of a null voltage is that the zero and the pole frequency become equal. By converse, the largest amplitude of the damping region is obtained in the limit case when $K_m = -K_{em}$, i.e. when the mechanical stiffness is equal to the negative stiffness of the electromagnet. In this case the equivalent stiffness and therefore the zero frequency are null. As a matter of fact, this last case is of little or no practical relevance as the system becomes marginally stable.
The equations governing the damping coefficient, the zero and electric pole (eq. (49) - eq. (51)) outline a design procedure of the damper for a given mechanical structure. Starting from the specifications, the procedure allows to compute the main parameters of the damper.

2.6.1 Specifications

The knowledge of (a) the resonant frequencies at which the dampers should be effective and (b) the maximum acceptable response allows to specify the needed value of the damping coefficient (*C*). The pole and zero frequencies (ω_{RL},ω_z) have be decided so as the relevant resonant frequencies fall within the damping range of the damper. Additionally, tolerance and construction technology considerations impose the nominal airgap thickness g_0. Electrical power supply considerations lead to the selection of the excitation voltage *V*.

2.6.2 Definition of the SAMD parametes

The mechanical stiffness K_m can be obtained from eq. (50) once the pole frequency (ω_{RL}) and the damping coefficient (*C*) are given by the specifications.

The electromechanical parameters of the damper: i.e. the electromechanical constant N^2A, and the total resistance *R* can be determined as follows:

a. the required electrical power V^2 / R is obtained from eq. (51). The knowledge of the available voltage *V* allows then to determine the resistance *R*.
b. The electromechanical constant N^2A is then found from eq. (48).

3. Experimental results

The present section is devoted to the experimental validation of the models described in section 2. Two different test benches were used. The former is devoted to validate the

models of the motional eddy current dampers while the latter is used to perform experimental tests on the transformer dampers in active mode (both in sensor and sensorless configuration), and semi-active mode.

3.1 Experimental validation of the motional eddy current dampers

The aim of the present section is to validate experimentally the model of the eddy current damper presented in section 2.3; in detail, the experimental work is addressed

- to confirm that the mechanical impedance ($Z_m(s)$) of a motional eddy current damper is given by the series of a viscous damper with damping coefficient c_{em} and a linear spring with stiffness k_{em} ,

c. to validate experimentally that the torque to constant speed characteristic ($T(\Omega)$) of a torsional damper operating as coupler or brake is described by the same parameters c_{em} c_{em} and k_{em} characterizing the mechanical impedance ($Z_m(s)$).

- to validate the correlation between the torque to speed characteristic and the mechanical impedance.

3.1.1 Induction machine used for the experimental tests

A four pole pairs (p = 4) axial flux induction machine has been realized for the steady state (Figure 9) and vibration tests (Figure 10). The magnetic flux is generated by permanent magnets while energy is dissipated in a solid conductive disk. The first array of 8 circular permanent magnets is bond on the iron disk (1) with alternate axial magnetization. The second array is bond on the disk (2) with the same criterion. Three calibrated pins (9) are used to face the two iron disk - permanent magnet assemblies ensuring a 1 mm airgap between the conductor and the magnet arrays. They are circumferentially oriented so that the magnets with opposite magnetization are faced to each other. In the following such an assembly is named "stator". The conductor disk (4) is placed in between the two arrays of magnets and is fixed to the shaft (6). It can rotate relative to the stator by means of two ball bearings installed in the hub (7 in Figure 10). Table 1 collects the main features of the induction machine.

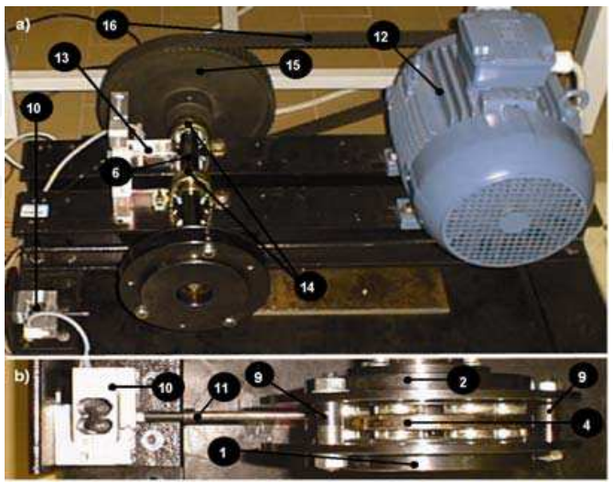

Fig. 9. Test rig used for the identification of the motional eddy current machine operating at steady state. a) View of the test rig. b) Zoom in the induction machine.

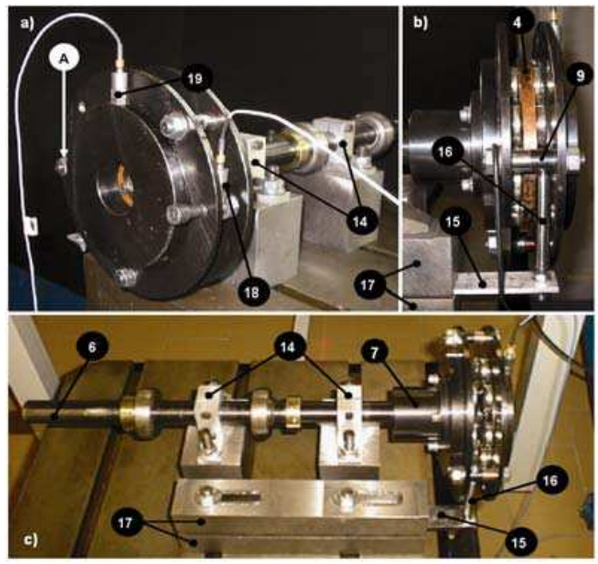

Fig. 10. Test rig configured for the vibration tests. a) Front, side view zoomed in the induction machine. The inpulse hammer force in applied at Point A. b) Lateral view of the induction machine. c) Top view of the whole test rig.

Feature	Unit	Value
Number of pole pairs	--	4
Diameter of the magnets	Mm	30
Thickness of the magnets	Mm	6
Magnets geometry	--	Circular
Magnets material	--	Nd–Fe–B (N45)
Residual magnetization of the magnets	T	1.22
Thickness of conductor	Mm	7
Conductivity of conductor (Cu)	$\Omega^{-1}m^{-1}$	$5.7x10^7$
Air gap	Mm	1

Table 1. Main features of the induction machine used for the tests.

3.1.2 Experimental characterization at steady state

The experimental tests at steady state were carried out to identify the slope c_0 of the torque to speed characteristic at zero or low speed and the pole frequency ω_p. Three type of tests, defined as "run up", "constant speed" and "quasi - static" have been carried out to this end.
Test rig set up (Figure 9). The electric motor (12 - asynchronous induction motor with rated power = 2.2 *kW*) drives the shaft (6) through the timing belt (16). The conductor disk (4) rotates with the shaft (6) being rigidly connected to it. The rotation of the stator is constrained by the bar (11) which connects one of the three pins of the stator to the load cell fixed to the basement. The tests at steady state are carried out by measuring the torque generated at different slip speeds Ω. The torque is obtained from the measurement of the tangential force while the slip speed Ω is measured using the pick up (13).

Run up tests. They are related to a set of speed ramps performed with constant acceleration. The ramp slopes have been chosen to ensure the steady state condition (a), the minimum temperature drift (b) and an enough time interval to acquire a significant amount of data (c). The rated power of the electric motor (12) limits the slip speed to 405 *rpm* that does not correspond to the maximum torque velocity ($\Omega_{T\max}$). Nevertheless, the inductive effects are evidenced allowing the identification of the electric pole ω_p (see Figure 11).
Constant Speed Tests. A second set of tests was carried out by measuring the counteracting torque with the induction machine rotating at a predefined constant slip speed. The aim is to increase the number of the data at low velocities where the run ups have not supplied enough points and to confirm the results acquired with the run up procedure.

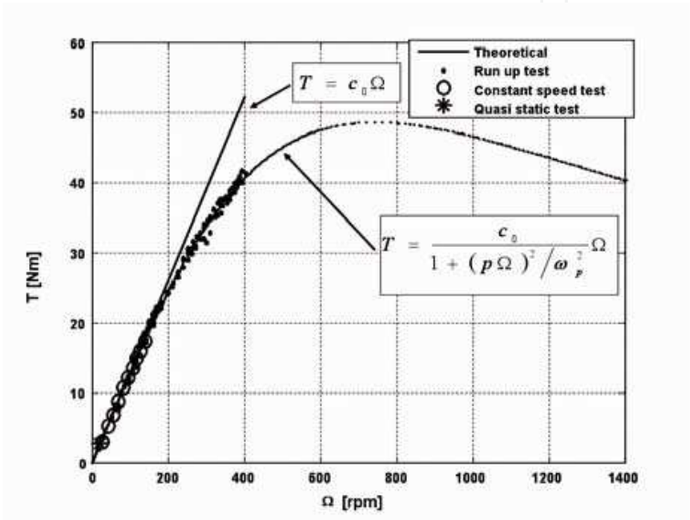

Fig. 11. Experimental results of the induction machine characterization at steady state.

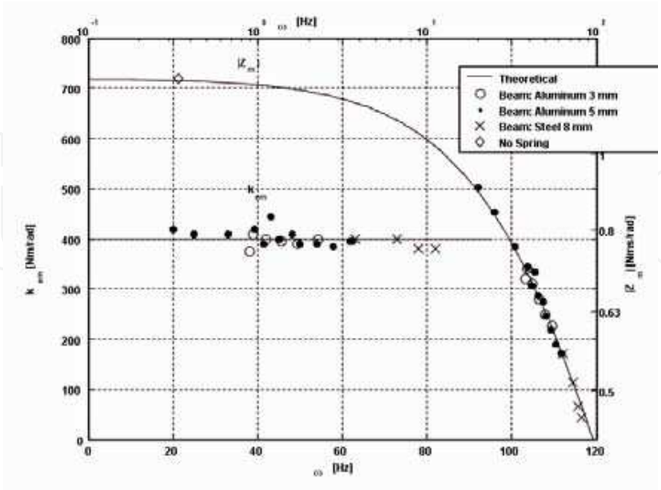

Fig. 12. Identified values of k_{em} in the frequency range 20–80 Hz. Full line, k_{em} mean value obtained as best fit of the experimental points. The experimental points of Z_m are plotted with reference to the top-right scale. Full line, Z_m plotted using $c_{em}=c_0$ and $k_{em} = \overline{k}_{em}$.

The results of the constant speed tests are plotted in the graph of Figure 11 with circle marks. Each point represents the average value of a set of 5 tests. The results are consistent with the expected trend and allow to get more experimental points at low speeds.

Quasi-Static Tests. The aim of the quasi static tests is to characterize the slope c_0 of the torque to speed curve at very low speed where eq.(28) reduces to $T = c_0\Omega$ (eq. (29)).

A motor driven test is not adequate for an accurate identification of c_0 as the inverter cannot control the electric motor at rotational speeds lower than 40 *rpm* The test set up was then modified locking the rotation of the shaft (6) connected to the conductor disk and enabling the rotation of the stator assembly. The driving torque was generated by a weight force (mg) acting tangentially on the stator. This is realized using a ballast (mass m) connected to a thread wound about the hub (7).

Under the assumption of low constant speed, the slope c_0 can be expressed as

$$c_0 = \frac{mg\Delta t}{\Delta x} r^2 \tag{52}$$

where Δt indicates the time interval required for the force mg to perform the work $L = mg\Delta x$ while r represents the radius of the hub ($m = 0.495\ kg,\ \Delta x = 1.54\ m,\ r = 32\ mm$). The tests have been carried out by measuring the time interval the ballast needs to cover the distance Δx. A set of 5 tests leads to an average slope $c_0 = 1.24\ \ Nms/rad$ (max deviation = 5%). The corresponding torque ($T_{quasi\_static} = 2.67\ \ Nm$ and speed ($\Omega_{quasi\_static} = 20.5$ rpm) are reported as the lowest experimental point (asterisk mark $*$) in the torque to speed curve of Figure 11. It agrees with the trend of the experimental data obtained at low speed during the motor driven tests.

Results of the Characterization at Steady State. The electric pole ω_p was identified as best fit of the experimental points reported in the graph of Figure 11 with the model of eq.(28). Being c_0 already known from the quasi static tests, the identified value of ω_p is

$$\omega_p = 51.1\,\text{Hz}, \qquad (c_0 = 1.24\,\text{Nms/rad})\,. \tag{53}$$

The full line curve plotted in Figure 11 was obtained using the identified values of c_0 and ω_p. The good correlation between the identified model and the experimental results can be considered as a proof of the validity of the steady state model in the investigated speed range. It derives that the maximum torque and the relative speed that characterize the induction machine operating at steady state are

$$T_{\max} = \frac{c_0\omega_p}{2p} = 49.8\text{Nm}, \qquad \Omega_{T\max} = \frac{\omega_p}{p} = 766\text{rpm}\,. \tag{54}$$

3.1.3 Vibration tests

The aim of the vibration tests is to validate experimentally the mechanical impedance of eq.(32) using the same induction machine adopted for the constant speed experimental characterization presented in section 3.1.2.

Test Rig set up. The test rig used for the steady state characterization was modified to realize a resonant system. The objective is to identify the parameters c_{em} and k_{em} from the response at the resonant frequency. To this end the rotation of the conductor disk (4 – Figure

10) was constrained by two rigid clamps (14) connected to the basement (a 300 kg seismic mass). The torsional spring is realized by a cantilever beam acting tangentially on the stator. Its free end is connected to one of the pins (9) by the axially rigid bar (16) while the constrained one is clamped by two steel blocks (17) bolted to the basement. The beam stiffness can be modified by varying its free length. This is obtained by sliding the blocks (17) relative to it. A set of three beams with different Young modulus and thickness (aluminum 3 and 5 *mm*, steel 8 *mm*) were used to cover the frequency range spanning from 20 *Hz* to 80 *Hz*. It's worth to note that the expected pole ω_p =52 *Hz* falls in the frequency range.

Impact tests using an instrumented hammer and two piezoelectric accelerometers were adopted to measure the frequency response between the tangential force (input) and the tangential accelerations (outputs), both applied and measured on the stator. Instrumented hammer and accelerometer signals are acquired and processed by a digital signal analyzer.

Identification Procedure. The identification of the electromechanical model parameters was carried out by the comparison of the numerical and experimental transfer function $T(s)/\dot{\theta}(s)$. The procedure leads to identify the damping coefficient c_{em} and the electrical pole ω_p (or the spring stiffness k_{em} being $\omega_p = k_{em}/c_{em}$) of the spring -damper series model of eq.(32). The value of the electromechanical damping obtained from the steady state characterization ($c_0 = 1.24 \quad Nms/rad$) is assumed to be valid also in dynamic vibration conditions ($c_{em} = c_0$). Even if this choice blends data coming from the static and the dynamic tests, it does not compromise the validity of the identification procedure and has been adopted to reduce the number of unknown parameters. Additionally it allows to perform the dynamic characterization by means of impact tests only. As a matter of fact, the best sensitivity for the identification of c_{em} could be obtained by setting the resonant frequency very low compared to the electrical pole (e.g. in the range of $\omega_p/10$). The values of the static damping, combined with low stiffness required in this case would imply a nearly critical damping of the resonant mode. This would make the impact test very unsuitable to excite the system.

The model used for the identification is characterized by a single degree of freedom torsional vibration system whose inertia is that of the stator ($J = \quad 0.033 \quad kgm^2$). The contribution of the cantilever beam and of the electromagnetic interaction are taken into account by a mechanical spring with structural damping $k_m(1+i\eta)$ in parallel to the spring - viscous damper series of electromagnetic stiffness k_{em} and electromagnetic damping c_{em}.

The procedure adopted for the identification is the following:

- Impact test without conductor disk to identify the mechanical spring stiffness k_m and the related structural damping η. This test is repeated for each resonance which is intended to be investigated.
- Assembly of the conductor disk. This step is carried out without modifying the set up of the bending spring whose stiffness k_m and damping η have been identified at the previous step.
- Impact test with conductor disk.
- Identification of the electromechanical stiffness k_{em} that allows the best fit between the numerical and experimental transfer function.

The procedure is repeated for 23 resonances in the frequency range 20-80 *Hz*. Figure 13 shows the comparison between the measured FRF and the transfer function of the identified model in the case of undamped (a) and damped (b) configuration at a resonance of 34 *Hz*.

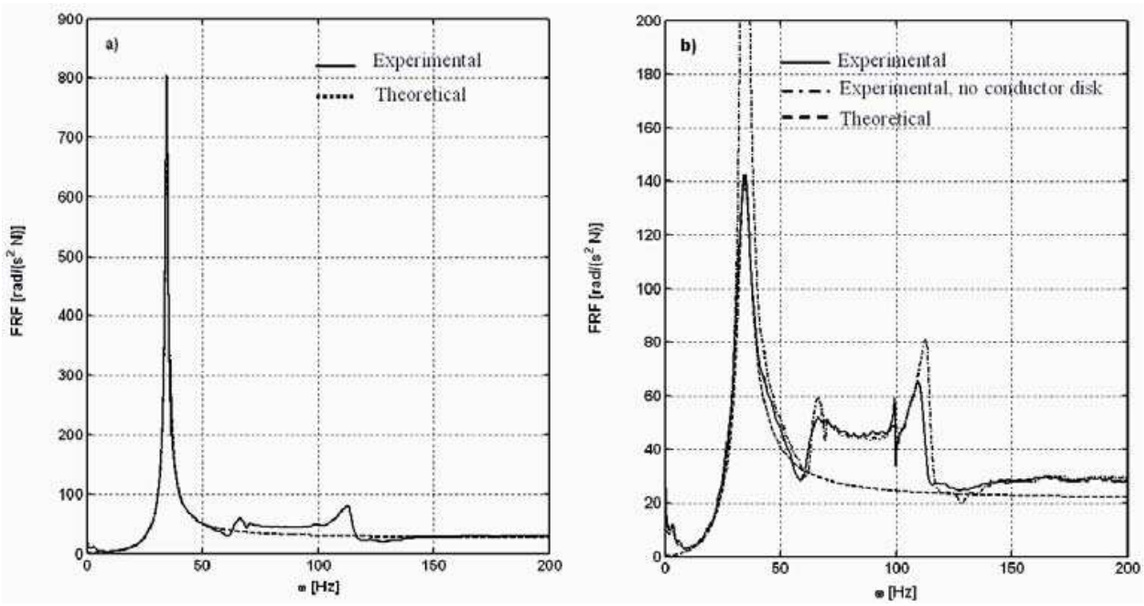

Fig. 13. Example of numerical and experimental FRF comparison. a) Identification of the torsional stiffness k_m and of the structural damping η b) Identification of k_{em} using for c_{em} the value obtained by the weight-driven tests (c_{em}=1.24 Nms/rad).

The close fit between the model and the experiments indicates that:

- the dynamic model and the relative identification procedure are satisfactory for the purpose of the present analysis.
- the differential setup adopted for the measurement (accelerations) eliminates the contribution of the flexural modes from the output response.
- the higher order dynamics (in the range 60 - 120 *Hz* for the resonance at 34 *Hz*) are probably due to a residual coupling that does not affect the identification of k_{em}. The comparison of the experimental curves in Figure 13b) highlights how the not modeled vibration motion influences the test with and without conductor disk in the same manner.

Figure 12 shows the results of the identification procedure. The values of the stiffness k_{em}, as identified in each test, are plotted as function of the relevant resonant frequency. Its mean value is

$$\bar{k}_{em} = 399.8\,\text{Nm/rad} \tag{55}$$

and is plotted as a full line. A standard deviation of 15.24 Nm/rad (3.8% of the mean value $\bar{k}_{em}$) is considered as a proof of the validity of the mechanical impedance model described by eq.(32). Adopting for c_{em} the damping obtained from the weight - driven test ($c_{em} = c_0 = 1.24$ Nms/rad) and for k_{em} the values identified by each vibration tests, the experimental points of Z_m, as reported in Figure 12, are obtained. The full line in the same graph refers to eq.(32) in which are adopted for c_{em} and k_{em} the following parameter: $c_{em} = c_0 = 1.24$ Nms/rad and $k_{em} = \bar{k}_{em} = 399.8$ Nm/rad. From that values it follows that the pole ω_p is

$$\omega_p = \bar{k}_{em} / c_{em} = 51.2\,\text{Hz} \tag{56}$$

The comparison proves the validity of the models. The small scattering of the experimental points about the mean value confirm the high predictability of the eddy current dampers and couplers with the operating conditions.

3.2 Experimental validation of the transformer dampers

Figure 14a shows the test rig used for the experimental characterization of the Transfomer dampers in active (sensor feedback (AMD) and self-sensing (SSAMD)) and semiactive (SAMD) configuration. It reproduces a single mechanical degree of freedom. A stiff aluminium arm is hinged to one end while the other end is connected to the moving part of the damper. The geometry adopted for the damper is the same of a heteropolar magnetic bearing. This leads to negligible stray fluxes, and makes the one-dimensional approximation acceptable for the analysis of the circuit.

The mechanical stiffness required to avoid instability is provided by additional springs. Two sets of three cylindrical coil springs are used to provide the arm with the required stiffness. They are preloaded with two screws that allow to adjust the equilibrium position of the arm. Attention has been paid to limit as much as possible to the friction in the hinge and between the springs and the base plates. To this end the hinge is realized with two roller bearings while the contact between the adjustment screws and the base plates is realized by means of steel balls. Mechanical stops limit to ± 5 degrees the oscillation of the arm relative to the centred position.

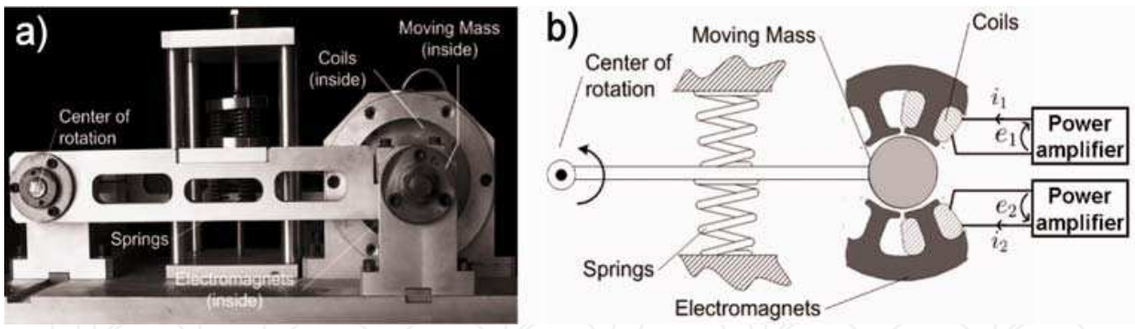

Fig. 14. a) Picture of the test rig b) Test rig scheme.

As shown in Figure 14b, the actuator coils are connected to the power amplifier. If it is simply a voltage supply, the system works in semi active mode while, when the power amplifier drives the coils as a current sink, the active configuration is obtained. If the current value is computed starting from the information of the position sensor, the damper works in sensor mode, otherwise, if the movement is estimated by using a technique as that described in section 2.5, the self-sensing operation is obtained.

3.2.1 Active Magnetic Damper (AMD)

When the Transformer damper is configured to operate in AMD mode, the position of the moving part is measured by means of an eddy current position sensors. Referring to Figure 15 the control system layout is completely decentralized.

Feature	Unit	Value
Damper- hinge distance	mm	320
Spring stiffness	N/m	6x30000
Hinge-spring system axis distance	mm	160
Magnetic circuit laminations	--	8 caves/4 electromagnets
Number of turns/electromagnet	--	142
Nominal air gap	mm	0.5
Air gap active area	mm²	420
Coil Resistance	Ω	0.4
Additional Resistance	Ω	1.0
Coil inductance at nominal air gap	mH	10.2

Table 2. Main features of the Transformer damper test bench.

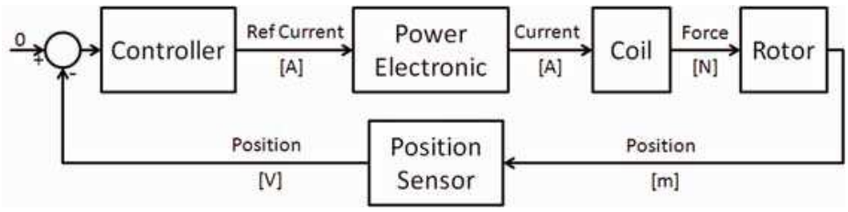

Fig. 15. Scheme of the complete control loop used in the AMD configuration.

The position signal is fed back into the corresponding controller and acts on the collocated electromagnet. The controller transfer function, capable to provide the required damping (by a simple PD control loop), is:

$$\frac{\mathrm{Re}\, f\ Current}{Position} = \frac{1.22 \cdot 10^{8}\,(s+13.25)}{(s+383.3)\,(s+1339)} \qquad \left[\frac{A}{m}\right] \tag{57}$$

The controller output is fed in the power electronic (full H-bridge switching) which current control loop assures an unitary gain and bandwidth@-3dB of about 1kHz.
The AMD and current loops are implemented on a DSP based electronic board.
The damping performances are evaluated comparing the time response of the closed-loop with the open-loop system when an impulse excitation is applied to the system. The impulse excitation is obtained by hitting the system with a hammer. In Figure 16, the open-loop system response (dashed line) is compared to the closed-loop one when the feedback controller, reported in eq.(57), is activated.

3.2.2 Self-Sensing Active Magnetic Damper (SSAMD)

The validation of the damper in self-sensing configuration was carried out by implementing in the DSP based electronic board used for AMD, the observer-controller described in section 2.5. The current flowing into the coils is measured by means of a hall current sensor and is fed back into the corresponding obserber-controller. The controller output acts on the collocated electromagnet. Observer and controllers parameters (poles) are reported in Table 3.

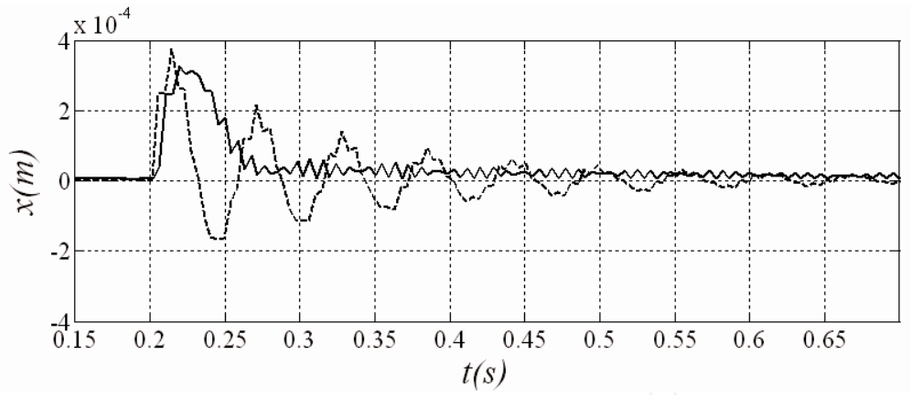

Fig. 16. Time response of the test rig to an impulse excitation. The time response of the system in two different configurations is plotted as follows: open-loop (dashed line) and closed-loop based with the AMD controller (solid line).

	Poles
Open Loop System	p_1=-3.32+113.35j
	p_2=-3.32-113.35j
	p_2=-62.6
Observer $eig(A-LC)$	p_1=-99.74+113.35j
	p_1=-99.74-113.35j
	p_2=-626.09
State-feedback controller $eig(A-BK)$	p_1=-29.92+109.38j
	p_1=-29.92-109.38j
	p_2=-500.87

Table 3. Main features of the Transformer damping in different control configuration.

The open-loop voltage-to-displacement transfer function obtained from the model and the experimental tests are compared in Figure 17a. The correspondence between the two plots is considered a good validation of the model. The same transfer functions in closed-loop operation with the controller designed in section 2.5 are compared in Figure 17b. Also in this case, the correspondence is quite good. This is a proof of the self sensing control strategy validity. The damping performances are evaluated by analyzing the time response of the closed-loop system when an impulse excitation is applied to the system.

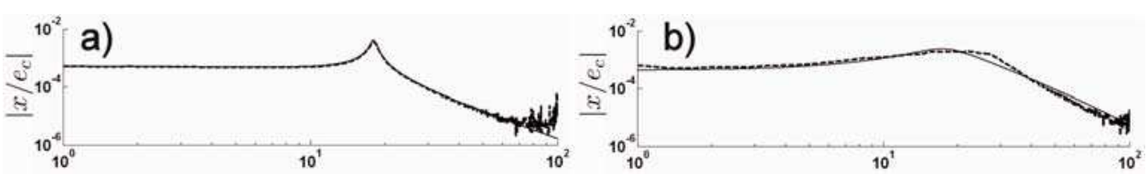

Fig. 17. Frequency response of the test rig in (a) open-loop and (b) closed-loop configuration compared to the model. Solid and dashed lines are the model and the plant frequency responses, respectively.

The impulse excitation is obtained by hitting the system with a hammer. In Figure 18, the open-loop system response (dashed line) is compared to the closed-loop one when the observer and state-feedback controller are designed from a model based on the nominal value of the system parameters. This result is worthy, as it shows that good damping can be achieved for active magnetic dampers obtained with the simplified model. Furthermore, this controller does not destabilize the system, as it is the case for full suspension self-sensing configurations.

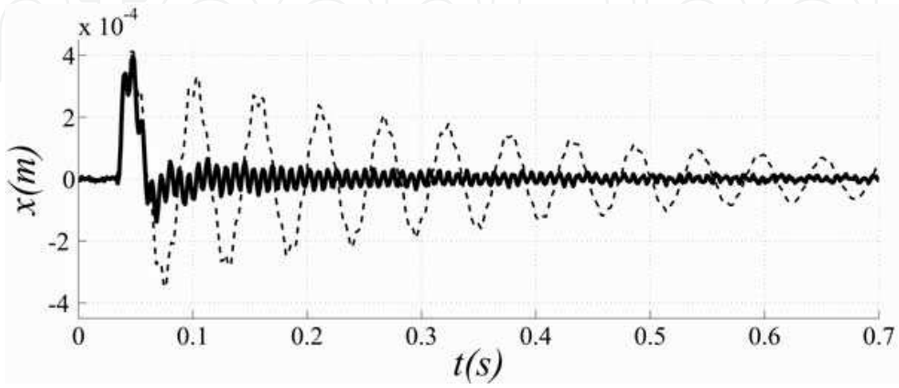

Fig. 18. Time response of the test rig to an impulse excitation. The time response of the system in two different configurations open-loop (dashed line) and closed-loop based on the identified model (solid line) is plotted.

3.2.3 Semi Active Magnetic Damper (SAMD)

As shown in the Figure 14b, the electrical terminals of each electromagnet are driven by a voltage power supply and (not shown) are connected in series to an additional resistance. The value of the additional resistance can be modified to tune the electrical pole frequency. The natural frequency of the mechanical system can be modified selecting coil spring with appropriate stiffness. During tests the mechanical frequency was set at 19 Hz and the electrical pole at 22.3 Hz. The main numerical parameters of the experimental set up are collected in Table 2.

The validation was performed by comparing the transfer function (FRF) between the input force and the output acceleration obtained from the experimental tests and that obtained from the model. The input force was actuated by means of an instrumented hammer; the acceleration was measured using an accelerometer. The impact point and the accelerometer are close to the end of the rigid arm. A first series of tests was performed with null excitation voltage.

The transfer functions obtained from the model are then compared in Figure 19a to the experimental ones for various excitation voltages.

Solid thick lines in the figure indicate the results from the model while the thin lines refer to the experimental results. The correlation between the numerical and experimental results confirms the validity of the adopted modelling approach and of the underlying assumptions.

As predicted by the model, increasing the voltage supply increases the damping range of the transformer damper. The modal damping is increased of a factor of about 20 from 0.0073

to 0.153 with a power expense of 1.4 W. Even if the damping is increased at the cost of a reduction of the resonant frequency, the large added damping demonstrates the effectiveness of the SAMDs. From the point of view of the required power the results obtained from the single degrees of freedom test bench demonstrates the need of electromagnets with small airgap and optimised geometry.
The non linear effects are also investigated. The system has been excited with impulse forces of increasing intensity and leaving constant the voltage supply. Impulse intensities are chosen so that the amplitude of the oscillation at the beginning of the transient are in a range 0.1-0.6 of the available airgap. The free oscillations due to different initial airgaps are reported in Figure 19b (voltage supply equal to 0.75 V). Higher displacements are not allowed due to the attractive force of the electromagnets that makes the system unstable.

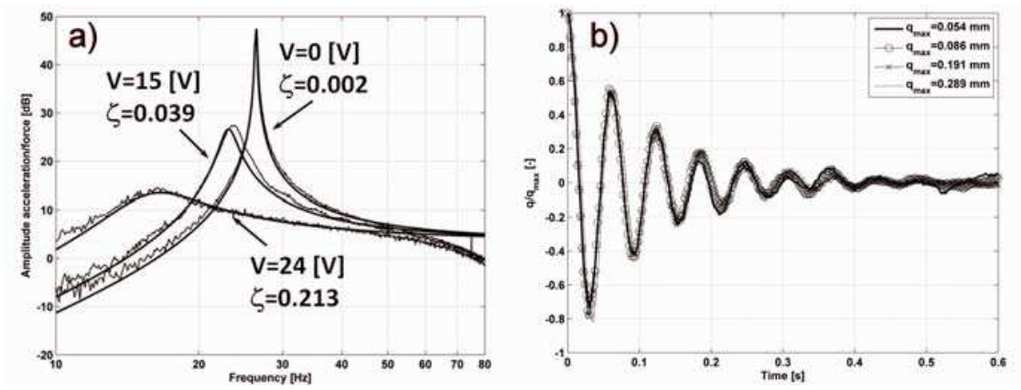

Fig. 19. a) Frequency response with various supply voltage for the SAMD b) Time response with various electromagnets airgaps for the SAMD.

4. Conclusions

The chapter describes the modelling and the experimental validation of different types of electromagnetic actuators used to damp the vibration in mechanical structures and machines. The first section describes the theoretical background based on an energetic approach. Section 2 is devoted to the description and analysis of possible configurations of electromagnetic actuators. The analysis is supported by the modelling of the different configurations. In section 3 the experimental validation is presented for four different types of damping devices: motional eddy current, transformer active based on sensor signal feedback, transformer active based on self sensing feedback and transformer semi-active.
The analyses described in the present chapter lead to the following results:

- the vibration response of a motiona eddy current damper can be modeled as the series connection of a linear mechanical spring and a viscous damper. In general an eddy current machine behaves as a crank whose end is connected to two spring/damper series acting along orthogonal directions.
- The mechanical impedance is a band limited function affected by the pole of the electric circuit. The band limitation can be usefully exploited in vibration isolation systems addressed either to reduce the vibration at the fundamental resonant frequency and to

minimize the transmissibility of higher excitation frequency. This feature is of interest also for eddy current couplers. A proper positioning of the electric pole allows to drive a load with a continuous torque filtering out the torque irregularities.

- The parameters describing the behavior of a motional eddy current damper are related to that of the same device operating at constant speed according to the "conversion rules" presented section 2.3.
- The technology of magnetic bearings can be adopted as damping systems if a mechanical element is introduced to stabilize statically the system. The static stability of the system allows the adoption of self sensing techniques to feedbach the state of the structure to be damped. It has been shown that the damping performance of the Luenberger observer based approach are comparable to the control strategies based on the position sensor feedback.
- Electromagnets as that adopted for magnetic bearings can be adopted also as passive or semi-active damping systems if a constant voltage is supplied to them. In section 1.6 it was shown that a mechanical impedance of a transformer damper parallel to a mechanical spring is characterized by a zero and a pole. At frequencies lower than the zero and higher than the pole, the device behaves as a mechanical spring. Between the zero and the pole, it operates as a pure viscous damper. The frequency of the pole can be tuned by adding an external resistance in series to the coil resistance.

5. References

Ahn, Y. K., Yang, B-S. & Morishita S. (2002). Directional Controllable Squeeze Film Damper Using Electro-Rheological Fluid, *ASME Journal of Vibration and Acoustics*, Vol. 124, pp. 105-109.

Crandall, S. H., Karnopp, D., Kurtz, E. F, Pridmore-Brown, E. C. (1968), *Dynamics of Mechanical and Electromechanical Systems*, New York: McGraw-Hill.

Genta, G. (2004), Dynamics of Rotating Systems, Springer Verlag.

Genta, G., Festini, A., De Lépine, X. (2008) From oil to magnetic fields: active and passive vibration control, *Acta mechanica et automatica*, 2(2), pp. 11-20.

Genta, G., Tonoli, A., Amati, N., Macchi, P., Silvagni, M., and Carabelli, S. (2006), More electric aeroengines: tradeoff between different electromagnetic dampers and supports, *Tenth International Symposium on Magnetic bearings*, EPFL, 21-23 Aug., Martigny, Switzerland.

Graves, K. E., Toncich, D., Iovenitti, P. G. (2000), Theoretical Comparison of the Motional and Transformer EMF Device Damping Efficiency, *Journal of Sound and Vibration*, Vol. 233, No. 3, pp 441-453.

Kamerbeek, E. M. H. (1973), *Electric motors'*, Philips tech. Rev., vol. 33, pp. 215--234.

Karnopp, D. (1989), Permanent Magnets Linear Motors used as Variable Mechanical Damper for Vehicle Suspension, *Vehicle System Dynamics*, Vol. 18, pp. 1 87-200.

Karnopp, D., Margolis, D. L., Rosenberg, R. C. (1990), *System Dynamics: a Unified Approach*, J. Wiley & Sons.

Kligerman, Y. , Gottlieb, O. (1998), Dynamics of a Rotating System with a Nonlinear Eddy-Current Damper, *ASME Journal of Vibration and Acoustics*, Vol. 120, pp. 848-853.

Kligerman, Y., Grushkevich, A., Darlow, M. S. (1998), Analytical and Experimental Evaluation of Instability in Rotordynamics System with Electromagnetic Eddy-Current Damper, *ASME Journal of Vibration and Acoustics*, Vol. 120, pp. 272-278.

Luenberger, D. G. (1971), An introduction to observers, IEEE *Trans. Autom. Contr*, AC-16(6), pp. 596-602.

Maslen, E., H., Montie, D., T., Iwasaki, T. (2006), Robustness limitations in self-sensing magnetic bearings, *Journal of Dynamic Systems, Measurement and Control*, 128, pp. 197-203.

Meisel, J. (1984), *Principles of Electromechanical Energy Conversion*, Robert Krieger, Malabar, Florida.

Mizuno, T., Araki, K., Bleuler, H., (1996), Stability analysis of self-sensing magnetic bearing controllers, IEEE *IEEE Transaction of Control System and Technology*, 4(5), pp. 572-579.

Mizuno, T., Namiki, H., Araki, K., (1996), Self-sensing operations of frequency-feedback magnetic bearings, *Fifth International Symposium on Magnetic Bearings*, 29-30 Aug., Kanazawa, Japan, pp. 119-123.

Mizuno, T., Ishii, T., Araki, K. (1998), Self-sensing magnetic suspension using hysteresis amplifier, *Cont. Eng. Pract.*, 6, pp. 1133-1140.

Nagaya, K. (1984), On a Magnetic Damper Consisting of a Circular Magnetic Flux and a Conductor of Arbitrary Shape. Part I: Derivation of the Damping Coefficients, *Journal of Dynamic Systems, Measurement and Control*, Vol. 106, pp. 46-51.

Nagaya, K. , Karube, Y. (1989), A Rotary Magnetic Damper or Brake Consisting of a Number of Sector Magnets and a Circular Conductor, *Journal of Dynamic Systems, Measurement and Control*, Vol. 111, pp. 97-104.

Noh, M. D., Maslen, E. H. (1997), Self-sensing magnetic bearings using parameter estimation, *IEEE Transaction of Instruments and Measurements*, 46(1), pp. 45-50.

Okada, Y., Matsuda, K., Nagai, B. (1992), Sensorless magnetic levitation control by measuring the PWM carrier frequency component, *Third International Symposium on Magnetic Bearings*, 21-31 July, Radisson Hotel, Alexandria, VA.

Schammass, A., Herzog, R., Buhler, P., Bleuler, H. (2005), New results for self-sensing active magnetic bearings using modulation approach, *IEEE Transaction of Control System and Technology*, 13(4), pp. 509-516.

Thibeault, N. M., Smith, R. (2002), Magnetic bearing measurement configurations and associated robustness and performance limitations, *Journal of Dynamic Systems, Measurement and Control*, 124, pp. 589-598.

Tonoli, A., Amati, N., Silvagni, M. (2008), Transformer eddy current dampers for the vibration control, *Journal of Dynamic Systems, Measurement and Control* , Vol. 130, pp. 031010-1 - 031010-9.

Vance, J. M. & Ying, D. (2000), Experimental Measurements of Actively Controlled Bearing Damping with an Electrorheological fluid, *ASME Journal of Engineering for Gas Turbines and Power*, Vol. 122, pp 337 - 344.

Vischer, D., and Bleuler, H. (1990), A new approach to sensorless and voltage controlled AMBs based on network theory concepts, *Second International Symposium on Magnetic bearings*, 12-14 July, Tokyo, Japan, pp. 301-306.

Vischer, D., Bleuler, H. (1993), Self-sensing magnetic levitation, *IEEE Transaction on Magnetics*, 29(2), pp. 1276-1281.

Tonoli A., Amati N., Bonfitto A., Silvagni M, Staples B., Karpenko E., (2010) - Design of Electromagnetic Dampers for Aero-Engine Applications, *Accepted for Journal of Engineering for Gas Turbines and Power*, ISSN: 0742-4795

Vibration Control

Edited by MickaÃƒÂ«l Lallart

ISBN 978-953-307-117-6
Hard cover, 380 pages
Publisher Sciyo
Published online 18, August, 2010
Published in print edition August, 2010

Vibrations are a part of our environment and daily life. Many of them are useful and are needed for many purposes, one of the best example being the hearing system. Nevertheless, vibrations are often undesirable and have to be suppressed or reduced, as they may be harmful to structures by generating damages or compromise the comfort of users through noise generation of mechanical wave transmission to the body. the purpose of this book is to present basic and advanced methods for efficiently controlling the vibrations and limiting their effects. Open-access publishing is an extraordinary opportunity for a wide dissemination of high quality research. This book is not an exception to this, and I am proud to introduce the works performed by experts from all over the world.

InTech Europe
University Campus STeP Ri
Slavka Krautzeka 83/A
51000 Rijeka, Croatia
Phone: +385 (51) 770 447
Fax: +385 (51) 686 166
www.intechopen.com

InTech China
Unit 405, Office Block, Hotel Equatorial Shanghai
No.65, Yan An Road (West), Shanghai, 200040, China
中国上海市延安西路65号上海国际贵都大饭店办公楼405单元
Phone: +86-21-62489820
Fax: +86-21-62489821

IntechOpen